Optically pumped quantum M_x–M_R magnetometer with high oscillating magnetic field*

Ding Zhi-Chao(丁志超)[a)b)], Yuan Jie(袁 杰)[a)b)†], Wang Zhi-Guo(汪之国)[a)b)‡]
Yang Kai-Yong(杨开勇)[a)b)], and Luo Hui(罗 晖)[a)b)]

[a)] College of Optoelectronic Science and Engineering, National University of Defense Technology, Changsha 410073, China
[b)] Interdisciplinary Center for Quantum Information, National University of Defense Technology, Changsha 410073, China

(Received 20 January 2015; revised manuscript received 9 March 2015; published online 20 June 2015)

A dip of the transverse component of the magnetic moment as a function of resonance frequency-detuning will emerge when the intensity of oscillating magnetic field exceeds a specific value, which is demonstrated theoretically and experimentally. The linewidth of magnetic-resonance signal can be much smaller than when the M_x–M_R magnetometer operates on condition that the intensity of oscillating magnetic field is smaller than this specific value, and the M_x–M_R magnetometer can possess a much higher signal-to-noise ratio. The experimental result shows that the sensitivity of M_x–M_R magnetometer can be improved by an order of magnitude under this condition.

Keywords: magnetic moment, linewidth, M_x–M_R magnetometer, sensitivity

PACS: 32.80.Xx, 07.55.Ge, 07.55.Jg **DOI:** 10.1088/1674-1056/24/8/083202

1. Introduction

Detection of a weak magnetic field is vital in many areas such as fundamental physics, biomagnetism, and geophysical exploration.[1–3] An optically pumped quantum magnetometer (OPQM) is excellent in these particular applications. The OPQM approach was first proposed by Dehmelt in 1957.[4] Later, it was implemented by Bloom.[5] After about five decades' development, great progress has been achieved.[6–8] The sensitivity of OPQM was demonstrated to be 15 fT/$\sqrt{\text{Hz}}$ in a spherical cell with a diameter of 7 cm and could reach 10 fT/$\sqrt{\text{Hz}}$ in the limit of shot noise.[6]

Based on the form of a magnetic resonance signal which is associated with the projection of the magnetic moment, general OPQMs are divided into M_z magnetometer and M_x magnetometer. The M_z magnetometer detects the absorption signal of the longitudinal component of the magnetic moment (M_z signal).[9] It possesses a relatively high sensitivity which is limited by the linewidth and signal-to-noise ratio but a slow response speed in the limit of longitudinal relaxation time T_1. The M_x magnetometer detects the phase of the oscillating transverse component of the magnetic moment (M_x signal).[9] Its response time is not limited by the relaxation time, so it possesses a high operational speed. However, it is so sensitive to the phase error that its sensitivity is relatively low. In many situations, a magnetometer with a high operational speed and sensitivity is necessary.[10] An idea of an M_x–M_z tandem which combines the advantages of M_z and M_x magnetometers was proposed and further developed.[11–13] It detects both the amplitude (M_R signal) and the phase of the oscillating transverse component of the magnetic moment. The M_R signal is similar to the M_z signal and also possesses high sensitivity but low operational speed which can be compensated for by the M_x signal.

As for the M_R magnetometer and M_z magnetometer, the sensitivity δB is given by

$$\delta B = \frac{\Delta\omega}{\gamma \times S_{\text{NR}}}, \tag{1}$$

where, $\Delta\omega$ is the resonance linewidth, γ is the gyromagnetic ratio of sensory atom (alkali-metal atom), and S_{NR} is the signal-to-noise ratio. So the sensitivity can be improved by reducing $\Delta\omega$ and improving S_{NR}. In a traditional measuring method, the Rabi frequency ω_1 satisfies

$$\omega_1 = \gamma B_1 \ll \frac{1}{\sqrt{T_1 T_2}}, \tag{2}$$

where, B_1 is the amplitude of oscillating magnetic field, and T_2 is the transverse relaxation time. Under this condition, the resonance linewidth is limited to $2/T_2$.

In this paper, a dip of the M_R signal as a function of resonance frequency-detuning will emerge when ω_1 is larger than $(T_1T_2)^{-1/2}$, which is demonstrated theoretically and experimentally. The M_x–M_R magnetometer which operates under this condition is analyzed. Compared with the M_x–M_R magnetometer which operates when $\omega_1 < (T_1T_2)^{-1/2}$ in Ref. [12], this magnetometer has a linewidth that can exceed the limit of $2/T_2$, and more important is that the M_x–M_R magnetometer can possess a much higher signal-to-noise ratio. When B_1 is

*Project supported by the National Natural Science Foundation of China (Grant No. 61475192) and the Science Research Program of National University of Defense Technology, China (Grant No. JC140702).

†Corresponding author. E-mail: jieyuan@nudt.edu.cn
‡Corresponding author. E-mail: maxborn@nudt.edu.cn

© 2015 Chinese Physical Society and IOP Publishing Ltd

properly chosen, the sensitivity can be improved by an order of magnitude. The M_x–M_R magnetometer with higher sensitivity can be achieved without losing the operational speed.

2. Theoretical computation

As for a vapor cell filled with alkali-metal atoms, considering a constant field B_0 directed along the Z axis in the laboratory coordinate system XYZ as shown in Fig. 1(a), the energy levels of alkali-metal atoms will split along the Z axis. In the equilibrium state, the numbers of atoms in different Zeeman energy levels obey the Boltzmann distribution, and it can be described by a macroscopic magnetization M_0 along the Z axis. As the difference in the number of atoms between different Zeeman energy levels is tiny, M_0 is quite small. If circularly polarized light is used to pump alkali-metal atoms along the Z axis,[14] M_0 will be improved by several orders of magnitude. In Fig. 1(a), an oscillating magnetic field $\boldsymbol{B}_1 = 2B_1\hat{x}\cos(\omega_a t)$ exciting the atomic transition is applied along the X axis.

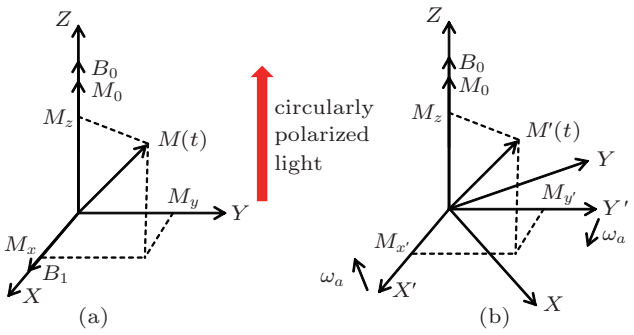


Fig. 1. (color online) Magnetization vectors in (a) a laboratory coordinate system XYZ and (b) a rotating coordinate system $X'Y'Z$.

A rotating coordinate system $X'Y'Z$ which rotates clockwise around the Z axis with a frequency of ω_α is introduced and shown in Fig. 1(b). The magnetization vector $\boldsymbol{M}$ due to spin polarization is represented as $(M_x(t),\ M_y(t),\ M_z(t))^{\mathrm{T}}$ in the XYZ coordinate system. In the $X'Y'Z$ coordinate system, the magnetization vector $\boldsymbol{M}'$ is represented as $(M_{x'}(t), M_{y'}(t), M_z(t))^{\mathrm{T}}$. The following relationship can be easily obtained:

$$\begin{aligned} M_x(t) &= M_{x'}(t)\cos(\omega_a t) + M_{y'}(t)\sin(\omega_a t) \\ &= M_R(t)\sin(\omega_a t) + \phi(t), \end{aligned} \tag{3}$$

in the above equation, $M_R(t) = \sqrt{M_{x'}(t)^2 + M_{y'}(t)^2}$, and $\phi(t) = \arctan\left(M_{x'}(t)/M_{y'}(t)\right)$.

For simplifying computation, we divide $\boldsymbol{B}_1$ into the clockwise components and counterclockwise components. The clockwise components are $B_x = B_1\cos(\omega_\alpha t)$ and $B_y = -B_1\sin(\omega_\alpha t)$, and the counterclockwise components are $B_x = B_1\cos(\omega_\alpha t)$ and $B_y = B_1\sin(\omega_\alpha t)$. The counterclockwise components have little influence on the evolution of $\boldsymbol{M}$ unless B_1 is quite large.[15] When we ignore the counterclockwise components with the rotating-wave approximation, the evolution of the magnetization vector $\boldsymbol{M}'$ can be described by

$$\begin{cases} \dfrac{\mathrm{d}M_{x'}(t)}{\mathrm{d}t} = \omega_2 M_{y'}(t) - \dfrac{M_{x'}(t)}{T_2}, \\ \dfrac{\mathrm{d}M_{y'}(t)}{\mathrm{d}t} = -\omega_2 M_{x'}(t) + \omega_1 M_z(t) - \dfrac{M_{y'}(t)}{T_2}, \\ \dfrac{\mathrm{d}M_z(t)}{\mathrm{d}t} = -\omega_1 M_{y'}(t) + \dfrac{M_0 - M_z(t)}{T_1}, \end{cases} \tag{4}$$

where, $\omega_2 = \gamma B_0 - \omega_\alpha$ is the detuning of resonance frequency. By setting the above equations to be equal to zero, the stationary solution can be obtained as follows:

$$\begin{cases} M_{x'} = M_0 \dfrac{\omega_2 T_2^2 \omega_1}{1 + (\omega_2 T_2)^2 + \omega_1^2 T_1 T_2}, \\ M_{y'} = M_0 \dfrac{T_2 \omega_1}{1 + (\omega_2 T_2)^2 + \omega_1^2 T_1 T_2}, \\ M_z = M_0 \dfrac{1 + (\omega_2 T_2)^2}{1 + (\omega_2 T_2)^2 + \omega_1^2 T_1 T_2}. \end{cases} \tag{5}$$

Substituting Eq. (5) into Eq. (3), we obtain

$$\begin{cases} M_R = M_0 \dfrac{T_2 \omega_1}{1 + (\omega_2 T_2)^2 + \omega_1^2 T_1 T_2} \sqrt{1 + (\omega_2 T_2)^2}, \\ \phi(t) = \arctan(\omega_2 T_2). \end{cases} \tag{6}$$

By setting $\mathrm{d}M_R/\mathrm{d}\omega_2 = 0$, the following solution can be easily obtained:

$$\omega_2\left[1 + (\omega_2 T_2)^2 - \omega_1^2 T_1 T_2\right] = 0. \tag{7}$$

If ω_1 is larger than $(T_1 T_2)^{-1/2}$, a dip of the M_R signal as a function of the resonance frequency-detuning emerges. The width of two peaks $\Delta\omega_{p-p}$ is

$$\Delta\omega_{p-p} = \frac{2}{T_2}\sqrt{\omega_1^2 T_1 T_2 - 1}. \tag{8}$$

Therefore, the linewidth (full-width at half-maximum) of the dip can exceed the limit of $2/T_2$.

When the influences of the counterclockwise components of $\boldsymbol{B}_1$ are considered, reference [15] shows that in the lowest order correction the shape of the resonance curve is unchanged but it is shifted. The resonance frequency (ω_0') is

$$\omega_0' = \omega_0\left[1 + \left(\frac{B_1}{2B_0}\right)^2\right]. \tag{9}$$

Here, $\omega_0 = \gamma B_0$, and $[B_1/(2B_0)]^2$ is the percentage of frequency-shift. Usually, $T_1 \approx 2T_2$.[16] By assuming $T_1 = 2T_2$, when $\omega_1^2 T_1 T_2 = 2$, $\omega_0[B_1/(2B_0)]^2 = 2/(8\omega_0 T_2 \times T_2)$. As for the usually used OPQMs, $8\omega_0 T_2$ is much larger than 1. So we can ignore the influence of the counterclockwise components. For achieving higher accuracy, we can also correct the resonance frequency by adding $\omega_0[B_1/(2B_0)]^2$.

3. Experimental setup

The experimental setup is shown in Fig. 2. A spherical Pyrex cell with a diameter of 2 cm contains ^{87}Rb atoms and 100 Torr (1.33322×10^2 Pa) of buffer gas (N_2 and ^{4}He) for slowing atomic diffusion and quenching. The cell is placed inside a five-layer magnetic shield and heated with a hot air oven. A constant magnetic field B_0 and an oscillating magnetic field B_1 are generated by the surrounding two pairs of Helmholtz coils. The Helmholtz coils along the Z axis are driven by steady current circuit and the Helmholtz coils along the X axis are driven by a lock-in amplifier. The pump beam is generated by a distributed feedback diode laser which is locked to ^{87}Rb D1 transition. It becomes circularly polarized beam after passing through a polaroid and $\lambda/4$ plate. Then, it polarizes the ^{87}Rb atoms along the Z axis after expansion and collimation. The probe beam is generated by a distributed feedback diode laser which is turned to near ^{87}Rb D1 transition. It illuminates the cell after passing through the polaroid and apparatus of expansion and collimation. The $M_x(t)$ signal is measured with a polarized beam splitter (PBS) and a balanced photodetector by utilizing optical rotation of the linearly polarized probe beam.[17] Finally, the detected signal is acquired and processed by the signal processing system.

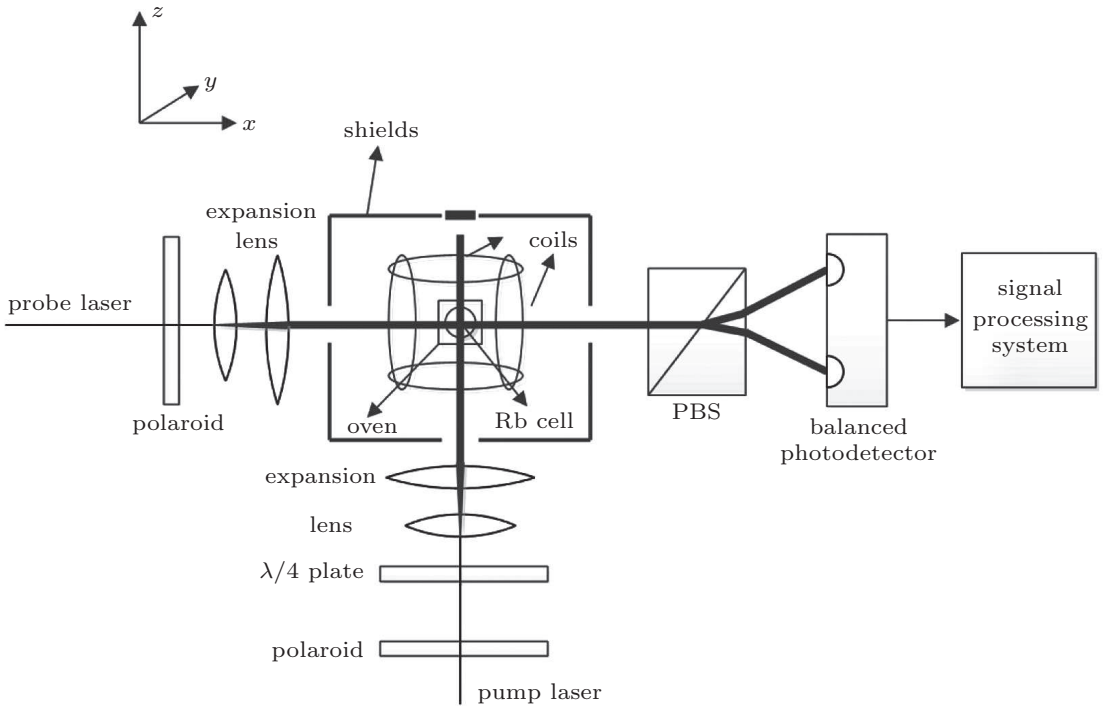


Fig. 2. Schematic diagram of the experimental setup.

4. Results and analysis

The cell is heated and its temperature is stabilized at 110 °C. The frequency of $\boldsymbol{B}_1$ is slowly linearly scanned with different amplitudes. The M_R signals are extracted from $M_x(t)$ signals and shown in Fig. 3 when $\omega_1 < (T_1T_2)^{-1/2}$ and $\omega_1 > (T_1T_2)^{-1/2}$. Compared with Fig. 3(a) when $\omega_1 < (T_1T_2)^{-1/2}$, figure 3(b) shows an obvious dip when $\omega_1 > (T_1T_2)^{-1/2}$.

In order to compare the characteristics of the M_x–M_R magnetometer when $\omega_1 < (T_1T_2)^{-1/2}$ with those when $\omega_1 > (T_1T_2)^{-1/2}$, we measure the sensitivities of the M_x–M_R magnetometer with different values of ω_1 under the same condition. When ω_1 is smaller than $(T_1T_2)^{-1/2}$, we define the resonance linewidth as the full-width at half-maximum of M_R signal, which is a function of detuning (ω_2), and the signal intensity as half of the amplitude of M_R at $\omega_2 = 0$. Similarly, when ω_1 is larger than $(T_1T_2)^{-1/2}$, the resonance linewidth is defined as the full-width at half-maximum of the dip and the signal intensity is defined as half of the depth of the dip. The experimental results of the linewidth and signal intensity as a function of ω_1 are shown in Figs. 4(a) and 4(b) by using asterisks. In Figs. 4 and 5, T_{20} is the transverse relaxation time which is obtained by measuring $\phi(t)$ as a function of ω_2 when ω_1 is much smaller than $(T_1T_2)^{-1/2}$,[18] and T_{10} is the longitudinal relaxation time which is assumed to be a constant. The computational results of the linewidth and signal intensity can be obtained from Eqs. (6) and (7) by assuming both T_2 and T_1 to be constants, which are shown in Figs. 4(a) and 4(b) by using solid lines. From Figs. 4(a) and 4(b), we can find that the results of experiment and computation are almost identical when ω_1 is small. As ω_1 becomes larger, the difference between experimental results and computational results increases. It is mainly because T_2 and T_1 are assumed to be constants in our

computation. In fact, T_2 is related to the intensity of oscillating magnetic field. The experimental results of T_2 are obtained at different values of ω_1 by measuring $\phi(t)$ as a function of ω_2, and the results are shown in Fig. 5. From Fig. 5, we can find that the influence of ω_1 on T_2 becomes much larger as ω_1 increases. Though T_2 is related to ω_1, the change in T_2 is less than forty percent. In addition, the operational speed of the M_x magnetometer is independent of relaxation time. Therefore, it has no influence on the operational speed of the M_x–M_R magnetometer.

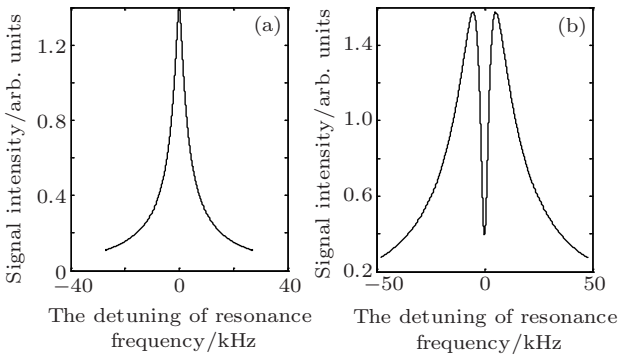


Fig. 3. The M_R signals extracted from $M_x(t)$ signals when (a) $\omega_1 < (T_1T_2)^{-1/2}$ and (b) $\omega_1 > (T_1T_2)^{-1/2}$.

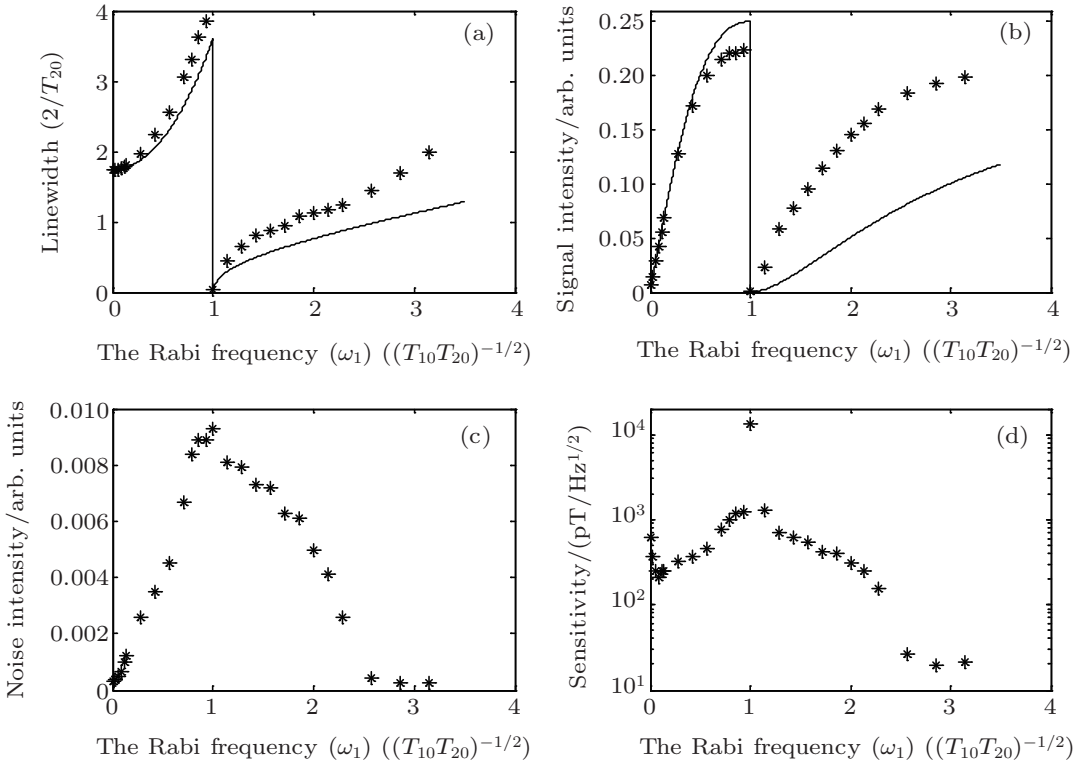


Fig. 4. Raw data of the resonance linewidth, the signal intensity, the noise intensity, and the sensitivity each as a function of ω_1. T_{20} is the transverse relaxation time which is obtained by measuring $\phi(t)$ as a function of ω_2 when ω_1 is much smaller than $(T_1T_2)^{-1/2}$, and T_{10} is the longitudinal relaxation time which is assumed to be a constant. (a) Experimental (asterisks) and computational (solid line) results of the resonance linewidth; (b) experimental (asterisks) and computational (solid line) results of the signal intensity; (c) experimental results of the noise intensity; (d) experimental results of the sensitivity.

Although the technical noises can be completely eliminated in theory, they dominate rather than the quantum noises in practice. As for the atomic magnetometer, there are many fluctuations which cannot be avoided, such as the fluctuations in frequency and intensity of pump laser and probe laser, temperature, etc. These fluctuations will induce the fluctuations (δM_0 and δT_2) in M_0 and T_2. When the noise intensity is defined by the fluctuation of the M_R signal at $\omega_2 = 0$, the intensities of these noises (N_{M0} and N_{T2}) induced by δM_0 and δT_2 can be obtained from Eq. (6) as follows:

$$\begin{cases} N_{M0} = \left|\dfrac{\partial M_R\,|\omega_2 = 0}{\partial M_0}\right| \delta M_0 = \dfrac{M_R\,|\omega_2 = 0}{M_0}\delta M_0, \\ N_{T2} = \left|\dfrac{\partial M_R\,|\omega_2 = 0}{\partial T_2}\right| \delta T_2 = \dfrac{(M_R\,|\omega_2 = 0)^2}{M_0 T_2^2 \omega_1}\delta T_2. \end{cases} \tag{10}$$

From the first expression of Eq. (10), it is easy to see that the noise intensity increases as the M_R signal at $\omega_2 = 0$ rises. From the second expression of Eq. (10), the noise intensity increases when the ratio of the square of the M_R signal at $\omega_2 = 0$ to ω_1 rises. According to the above definition of the signal intensity, when ω_1 is smaller than $(T_1T_2)^{-1/2}$, the signal intensity is positively associated with the M_R signal at $\omega_2 = 0$. However, when ω_1 is larger than $(T_1T_2)^{-1/2}$, the signal

intensity is negatively associated with the M_R signal at $\omega_2 = 0$. From Eq. (6), the M_R signal at $\omega_2 = 0$ reaches a maximum at $\omega_1 = (T_1T_2)^{-1/2}$ and will decrease when $\omega_1 > (T_1T_2)^{-1/2}$. Considering these conditions, the noise intensity as a function of ω_1 first increases, and then decreases. The noise intensity is large when the signal intensity is large under the condition of $\omega_1 < (T_1T_2)^{-1/2}$. On the contrary, the noise intensity is small when the signal intensity is large under the condition of $\omega_1 > (T_1T_2)^{-1/2}$. For obtaining the noise intensity experimentally, the M_R signal at $\omega_2 = 0$ passes through a low-pass filter with a cut-off frequency of 50 Hz, and then the filtered signals are continually acquired. By computing the standard deviation of 1000 continual data of the acquired M_R signal intensity at $\omega_2 = 0$, the noise intensity with a bandwidth of 50 Hz is obtained and shown in Fig. 4(c). From Figs. 4(b) and 4(c), we can find that the M_x–M_R magnetometer can possess a strong anti-noise ability and its signal-to-noise ratio can be much larger when $\omega_1 > (T_1T_2)^{-1/2}$ than when $\omega_1 < (T_1T_2)^{-1/2}$.

The sensitivity can be computed by utilizing Eq. (1), and the result is shown in Fig. 4(d). Under our experimental condition, the sensitivity of the M_x–M_R magnetometer can be improved by an order of magnitude when $\omega_1 > (T_1T_2)^{-1/2}$ compared with when $\omega_1 < (T_1T_2)^{-1/2}$.

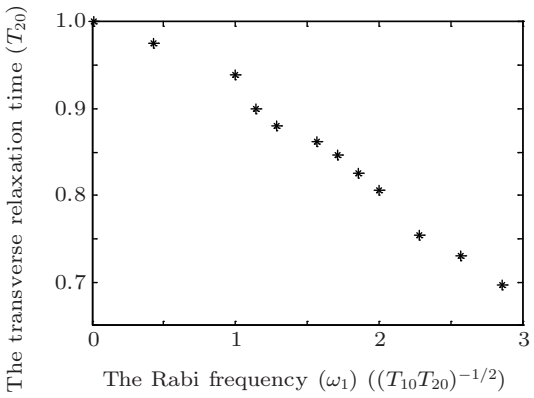


Fig. 5. Raw data of the transverse relaxation time as a function of ω_1.

5. Conclusions

In this study, a dip of the M_R signal will emerge when the Rabi frequency is larger than $(T_1T_2)^{-1/2}$, which has been analyzed. The resonance linewidth of the dip can exceed the limit of $2/T_2$. The experimental result shows that the oscillating magnetic field has an influence on transverse relaxation time and the influence becomes much larger as the intensity of oscillating magnetic field increases. However, the operational speed of the M_x magnetometer is independent of relaxation time. So the intensity of oscillating magnetic field has no influence on the operational speed of the M_x–M_R magnetometer. It is demonstrated theoretically and experimentally that the noise intensity is large when the signal intensity is large under the condition of $\omega_1 < (T_1T_2)^{-1/2}$. On the contrary, the noise intensity is small when the signal intensity is large under the condition of $\omega_1 > (T_1T_2)^{-1/2}$. Therefore, the M_x–M_R magnetometer can possess a strong anti-noise ability and its signal-to-noise ratio can be much larger when $\omega_1 > (T_1T_2)^{-1/2}$. Its sensitivity can be improved by an order of magnitude without losing the operational speed under our experimental condition. Further research is needed to further improve the characteristics and solve some open problems.

References

[1] Brown J M, Smullin S J, Kornack T W and Romalis M V 2010 *Phys. Rev. Lett.* **105** 151604
[2] Johnson C, Schwindt P D D and Weisend M 2010 *Appl. Phys. Lett.* **97** 243703
[3] Mathéa V, Lévêquea F, Mathéb P E, Chevallierc C and Ponsc Y 2006 *Appl. Geophys.* **58** 202
[4] Dehmelt H G 1957 *Phys. Rev.* **105** 1487
[5] Bloom A L 1962 *Appl. Opt.* **1** 61
[6] Groeger S, Bison G, Schenker J L, Wynands R and Weis A 2006 *Eur. Phys. J. D* **38** 239
[7] Huang K K, Li N and Lu X H 2012 *Chin. Phys. Lett.* **29** 100701
[8] Gu Y, Shi R Y and Wang Y H 2014 *Acta. Phys. Sin.* **63** 110701 (in Chinese)
[9] Aleksandrov E B and Vershovskii A K 2009 *Phys. Uspekhi* **52** 573
[10] Billings S D 2004 *IEEE Trans. Geosci. Remote Sens.* **42** 1241
[11] Vershovskii A K and Pazgalev A S 2011 *Tech. Phys. Lett.* **37** 23
[12] Vershovskii A K, Dmitriev S P and Pazgalev A S 2013 *Tech. Phys.* **58** 1481
[13] Vershovskii A K, Pazgalev A S and Alexandrov E B 2014 *Laser Phys.* **24** 074017
[14] Happer W 1972 *Rev. Mod. Phys.* **44** 169
[15] Bloch F and Siegert A 1940 *Phys. Rev.* **57** 522
[16] Cates G D, Schaefer S R and Happer W 1998 *Phys. Rev. A* **37** 2877
[17] Budker D, Gawlik W, Kimball D F, Rochester S M, Yashchuk V V and Weis A 2002 *Rev. Mod. Phys.* **74** 1153
[18] Terao A, Ban K, Ichihara S, Mizutani N and Kobayashi T 2013 *Phys. Rev. A* **88** 063413